Low loss, high-speed single-mode half-disk resonator

Xinbai Li, Qingzhong Deng, and Zhiping Zhou*

State Key Laboratory of Advanced Optical Communication Systems and Networks, School of Electronics Engineering and Computer Science, Peking University, Beijing, 100871, China

**Corresponding author: zjzhou@pku.edu.cn*

Received February 24, 2014; accepted May 11, 2014;
posted May 22, 2014 (Doc. ID 207018); published June 20, 2014

This work proposes a new type of resonator: a single-mode half-disk resonator. Half of the resonator is solid, allowing large electrical or mechanical contacts, and a single-mode operation can be retained. A systematic design method is demonstrated and analyzed. For a 3 μm radius, the simulation predicts an internal Q-factor as high as 2.4×10^5, and a loaded Q-factor of ~9000 is measured in experiments, comparable even with uncontacted microrings of bigger radii. The large contacts will improve the performance of a wide range of active devices. We present the contact resistance of a vertical PN junction modulator based on this structure, which can be reduced to nearly an order of magnitude, enabling a much faster modulation speed.

OCIS codes: (130.0130) Integrated optics; (130.3120) Integrated optics devices.
http://dx.doi.org/10.1364/OL.39.003810

The requirements of future computation and communication systems have put a stringent energy budget on silicon photonics interconnect circuits. For modulators, the energy consumption should be lower than 10 fJ/bit in high-speed modulation [1,2]. Vertical PN junction modulators have the highest modulation efficiency among all junction types, about 1/16 the energy consumption of a lateral PN junction, and vertical design keeps a record of the lowest energy consumption of only 3 fJ/bit [3]. However, a major problem for vertical PN junction lies in designing electrical contacts, because any contact on a ring waveguide will cause substantial scattering loss. Recently, adiabatic microring resonator (AMR) has been proposed to solve this problem [4,5], achieving interior electrical contacts without causing considerable leak of the optical field as in the case of microring. However, contacts are limited to a small area in the AMR. For modulators, this leads to a large contact resistance and RC-limited bandwidth, especially in small radius rings where photon lifetime plays a less significant role. Besides modulators, resonators capable of low-loss large contacts can find extensive applications in optical interconnection and communication [6–8]. Filters, switches, and multiplexers with active tuning/controlling will benefit from higher efficiency, speed, and Q-factor.

In the field of microdisks, multiple geometrical modifications have been reported in an attempt to achieve single-mode or mode reduction, e.g., gear-shaped [9], hole-piercing [10]. Nevertheless, single-mode is still out of reach with a completely solid disk. The idea of this Letter stems from the low-loss feature of microdisks, that is, to loosen the confinement of the whispering gallery mode (WGM) as much as possible.

In this work, we propose a class of single-mode half-disk resonators (HDRs) that maintain a high Q-factor even when half of the resonator is available for contacts. It is aimed to expand the available area of electrical or mechanical contacts, reducing loss, and facilitating a much higher speed. A systematic and generalized design method is demonstrated. Simulations and experiments are performed to verify this method.

The HDR has the advantage of the WGM, which can propagate without confinement from inner boundary, making it possible to travel through the contact area without leakage. Figure 1(a) illustrates the structure of the proposed device. The gray and white areas stand for silicon and SiO_2, respectively. The vertical dotted line represents the axis of symmetry. The ring waveguide is narrow at the coupling region (bottom) to ensure single-mode coupling, and gradually widens, loosening the confinement of the WGM. Apparently, a widening too abrupt will cause greater transitional loss or multimode. The contact area is where electrical or mechanical contacts can be made.

In order to design a smooth transition curve to reduce transitional loss, the minimum variation curve is modified, which is an interpolation curve that minimizes the L^2-norm of curvature variation [11]. At the endpoint of the total arc length s_1, the transition curve satisfies G2 continuity to form smooth joints:

$$\begin{aligned} \kappa_1(s_1) &= \kappa_2(s_1), \\ \theta_1(s_1) &= \theta_2(s_1), \\ \frac{d\kappa_1}{ds}(s_1) &= \frac{d\kappa_2}{ds}(s_1) = 0, \end{aligned} \tag{1}$$

where $\kappa(s)$ and $\theta(s)$ represent the curvature and tangent angles of the curve, and s_1 stands for the total length of

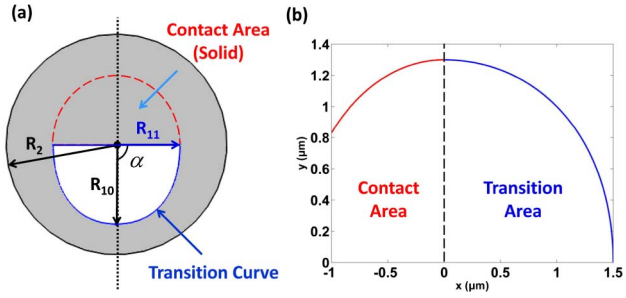

Fig. 1. (a) Schematic of a single-mode HDR. Light inputs from the bus waveguide and evanescently couples to the HDR coupling region at the bottom. The gray and white areas represent silicon and SiO_2, respectively. (b) Demonstration of 90° transition curve design, $R_{11} = 1.3$ μm, $R_2 = 2$ μm, showing a smooth joint between contact area and transition area.

the curve. For clarity, we establish a Cartesian coordinate with origin at the center of the cavity, as shown in Fig. 1(b). Consider that the transition curve starts at point (R_{10}, 0) and ends at point ($R_{11}\cos\alpha$, $R_{11}\sin\alpha$). The curvature κ can be well approximated by the third-order polynomial [11,12]:

$$\kappa(s) = \frac{1}{R_{10}} + a_1 s + a_2 s^2 + a_3 s^3,$$
$$\theta(s) = \frac{\pi}{2} + \frac{1}{R_{10}} s + \frac{a_1}{2} s^2 + \frac{a_2}{3} s^3 + \frac{a_3}{4} s^4. \quad (2)$$

The transformation from arc length s to a Cartesian coordinate x, y can be realized by an iterative method:

$$x_i = x_{i-1} + \cos[\theta((i-1)ds)]ds,$$
$$y_i = y_{i-1} + \sin[\theta((i-1)ds)]ds. \quad (3)$$

Curve parameters a_1, a_2, a_3, s_1 are solutions of the above Eq. (1–3). Combining Eq. (1) and Eq. (2) yields the following boundary conditions:

$$\theta(s_1) = \frac{\pi}{2} + \alpha,$$
$$\frac{d\kappa}{ds}(s_1) = 0,$$
$$x_n = R_{11}\cos\alpha,$$
$$y_n = R_{11}\sin\alpha, \quad (4)$$

where α stands for the central angle of the transition curve, fixed at 90° in our design.

To summarize the design procedures, first the parameter $R_{10} = R_2 - W$ (R_2, outer radius, W, waveguide width at coupling region) is determined according to the acceptable coupling gap. For example, $R_2 = 3$ μm rings usually have $W \le 400$ nm for a coupling gap wider than 200 nm. Next, solve Eq. (4) of a different preset, R_{11}, and obtain the curves in a Cartesian coordinate using Eq. (3). Finally, optimize single parameter R_{11} to achieve the best performance. This generalized method has proven to be valid on arbitrary parameter combinations.

The design of the $R_2 = 2$ μm transition curve is demonstrated, in which half of the HDR is available for contacts, with an inner radius of $R_{11} = 1.3$ μm, $R_{10} = 1.5$ μm. Results are shown in Fig. 1(b), with the blue line (right being the transition curve, and the red line (left) being the circular arc of contact area connecting with it. From the figure, the G2 continuity conditions ensure a smooth joint at $x = 0$ and prevent mode conversion at endpoints. Here we note that, although the circular boundary of contact area does not exist in the real device [Fig. 2(a)], the continuity conditions ensure smoothness even when the contact area is doped or filled with other materials. In addition, the proposed design method is based on equation-solving and hence can be very robust and time-efficient, facilitating R_{11} optimization.

2D simulations are performed to prove the design concept, determine internal Q-factor, and optimize the parameter R_{11}. A 220-nm thick silicon HDR surrounded by an SiO_2 is analyzed at a 1550 nm wavelength. Figure 2(a) depicts the light field distribution in the HDR. It is clearly seen that no leaky modes or higher order modes are generated; thus single-mode operation can be achieved by this device. Although the WGM has a larger mode volume than the strongly confined guided mode at the coupling region, there is no field distribution in the contact area. Therefore, electrical contacts fabricated in the center do not interact with the light field, and thereby induce no extra loss, whether highly doped or covered with metal electrode. Figure 2(b) shows the optimization of the parameter R_{11}; here $R_{10} = 1.6$ μm is considered to allow a wider coupling gap. The optimal value is around $R_{11} = 1.35$ μm, achieving an internal Q-factor as high as 1×10^5. For the $R_2 = 3$ μm case, an internal Q-factor has a similar relationship with R_{11}, but peaks at $R_{11} = 2.2$ μm with an internal Q-factor of 2.4×10^5.

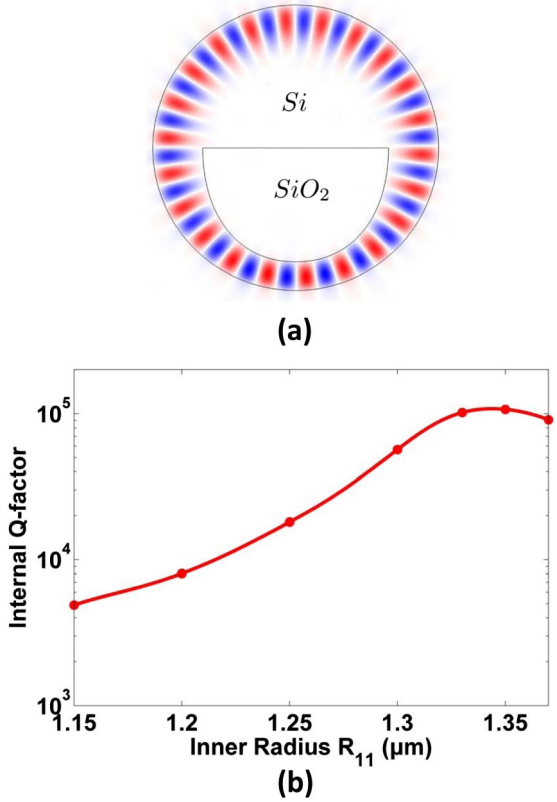

Fig. 2. (a) Proof of concept: field distribution of the 2D-Finite element method (FEM) simulation of the HDR with 180° contact. Only a fundamental mode is supported and no field distribution occurs in the center. (b) 2D-FEM optimization of the internal Q-factor versus different R_{11}, $R_{10} = 1.6$ μm, $R_2 = 2$ μm. A high internal Q-factor of 10^5 can be maintained despite large contact.

The internal Q-factor is a figure of merit that directly reflects the loss feature of the resonator. The simulated internal Q-factor is higher than the AMR (88,000, 2D simulation, [4]) while our device allows a much larger contact area. It is enlightening that a lower loss is not realized by tightly shaping and confining the WGM, but by loosening its confinement as much as possible outside the coupling region. Additionally, for a fabrication error of ±20 nm around optimal R_{11}, the internal Q-factor

shows less than a 10% variation, indicating good tolerance.

The HDR in this work is fabricated on a 220-nm-thick silicon-on-insulator (SOI) platform with a 2-μm buried oxide layer. The E-beam is used to define the pattern. After inductively coupled plasma (ICP) etching, a 1-μm thick plasma-enhanced chemical vapor deposition (PECVD) silicon oxide is deposited on top. The HDR has an outer radius of $R_2 = 3$ μm and an inner radius of $R_{11} = 2.2$ μm. In the coupling region, both the bus waveguide and the ring waveguide have a width of 400 nm, and the coupling gap is 240 nm (critical coupling). A scanning electron microscope (SEM) image of the fabricated device is shown in Fig. 3. The etching selectivity is not as good as we expected, resulting in a straight waveguide and a ring waveguide width of ~370 nm in coupling region. This increases the cavity loss and makes the HDR slightly over-coupled. The measured R_{11} has a +35 nm deviation from an optimal value of 2.2 μm, and although a single-mode operation will be retained, it compresses the WGM mode volume and thus reduces the Q-factor. Figure 3(b) shows the magnified view of the transition area, marked in Fig. 3(a). Small corrugations can be seen on the waveguide transition area, possibly caused by nonuniformity of the etching process. The following measurements, though, indicate our device can tolerate small unsmooth corrugations without major degradation of performance.

For the characterization of the fabricated HDR, a tunable laser is used as the light source in our measurement system and butt-coupled to the chip with a tapered fiber. The optical transmission spectrum is measured as shown in Fig. 4, achieving a 36 nm uncorrupted free spectral range (FSR) and loaded Q-factor of ~9000. Generally, a loaded Q-factor is directly measurable in experiment and is substantially lower than the internal Q-factor because of the coupling loss, coupling conditions, etc. Some published results are listed here for references: the internal Q-factor of the 5 μm radius conventional microring resonator far exceeds 10^6, but a loaded Q-factor of fabricated is usually around 10,000–20,000 (doped, [13], undoped [14]). For small rings, the 1.5 μm radius possesses an internal and loaded Q-factor of 46,000 and 3000, respectively [15]. It is clear that the proposed device has an outstanding low-loss feature, even comparable with uncontacted microrings of bigger radii. The clean optical spectrum free of multi-mode resonances

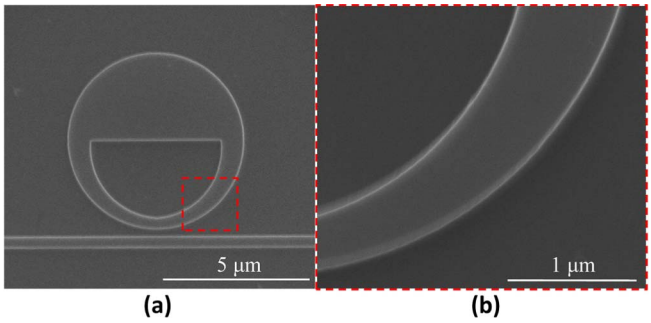

Fig. 3. (a) SEM image of single-mode HDR. (b) Magnified view of transition area marked in (a). The fabricated parameter deviates from the optimal value. Finer fabrication will further improve its performance.

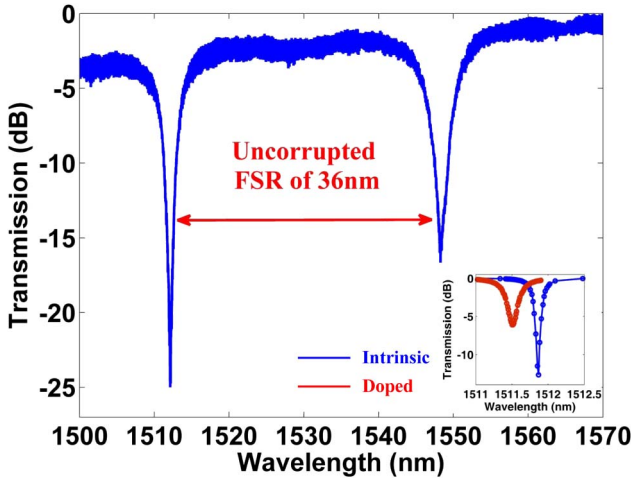

Fig. 4. Optical transmission spectrum. The lack of multimode resonance peaks confirm single-mode operation. The loaded Q-factor of ~9000 is measured at a 1512 nm peak. The inset shows a 3D-FEM simulation of intrinsic (right) and doped (left) HDR transmission spectra according to parameters measured in SEM photographs. The waveguide is 370 nm wide and the coupling gap is 249 nm. Loaded Q-factors of 10,132 and 6090 are obtained for intrinsic and doped HDR, respectively. Surface roughness is not considered in the simulation.

indicates a single-mode operation, in accordance with the simulation results in Fig. 2(a), verifying the competence of the proposed method.

In order to compare the simulation and experiment results, a 3D-FEM simulation of the HDR transmission under the exact structural parameters measured in SEM photographs is provided in the Fig. 4 inset. The resonant wavelength of the intrinsic HDR is simulated to be 1512 nm (blue curve on the right), with a loaded Q-factor of 10,132. The resonant wavelength is in accurate accordance with the experiment results, and the Q-factor is only slightly higher because surface roughness is not included in simulation. This consistency allows further accurate analysis of the doping impact. The red curve on the left illustrates full doping of the HDR at $1 \times 10^{18}/\text{cm}^3$ at the same coupling gap. The loaded Q-factor is measured to be 6090 as a result of free carrier absorption.

The main purpose of this work is to propose a low-loss single-mode HDR that allows larger contacts. To better present its capabilities, a schematic of a vertical junction modulator based on the HDR is supplemented as shown in Fig. 5. Enabled by the HDR's features, the presented electrical contact design is the widest direct contact of the single-mode modulator. The doping concentration for P and N type is $1 \times 10^{18}/\text{cm}^3$, a trade-off between modulation efficiency and absorption loss. T 60 nm-thick intrinsic silicon between P+ and N+ layers can avoid forming a P+/N+ junction. The validity of the same doping concentration vertical PN junction modulators has been reported in several studies [3,5]. Since the innovation of Fig. 5 is in a contact area, only characteristics relevant to modulation speed are analyzed below. P/N doping will induce additional ~3 dB/mm loss, and the corresponding intrinsic Q-factor will be reduced to around 20,000, deduced from the loss-Q relations [15].

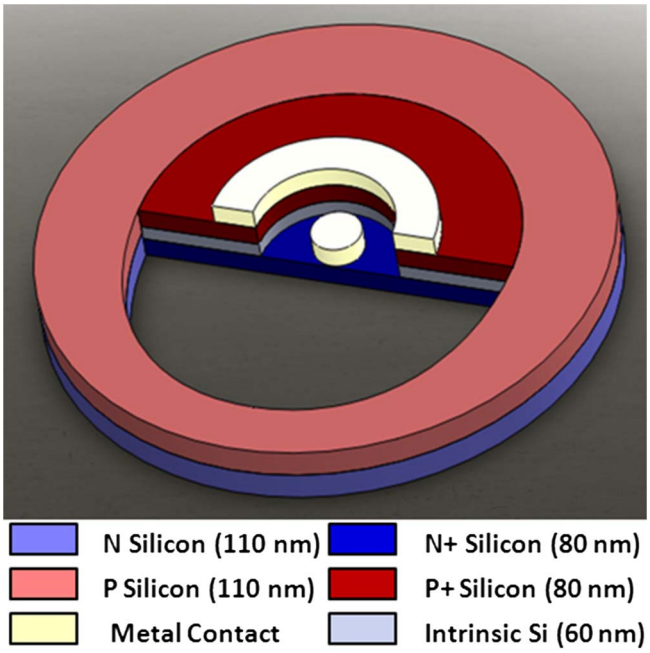

Fig. 5. Schematic of the vertical PN junction modulator based on the HDR. A large contact area greatly reduces resistance, thus increasing the RC-limited bandwidth.

As illustrated in the Fig. 4 inset, the loaded Q-factor decreases to 6090 after doping. A reference to this is AMR of full and partial doping has loaded Q-factor of 2874, 3281, respectively [5]. Therefore, the HDR will be well functional after doping. The uniqueness of the proposed schematic lies in the wide direct contact enabled by the HDR. According to the 3D-FEM simulation, resistance of the device is ~50 Ω. For comparison, AMRs with silicon contacts of a 200 or 400 nm width have a resistance of about 550 and 400 Ω, respectively. The considerable reduction in resistance can be explained by a contact area that is about 15 times larger. The depletion capacitance of the PN junction satisfies Eq. (5).

$$C(V) = A\sqrt{\frac{\varepsilon_r \varepsilon_0 q N_A N_D}{2(N_A + N_D)(V - \phi_B)}}, \tag{5}$$

where A is the total cross-section area of the junction, $\varepsilon_r\varepsilon_0$ is the dielectric constant of silicon, q is the elementary charge, N_A and N_D are the doping concentration of P type and N type, and V and φ_B are the reverse bias voltage and built-in potential. The device capacitance is calculated to be ~20 fF. The total modulation speed is constrained by the photon lifetime τ and electrical characteristics, primarily the RC constant in this lumped device. With a loaded Q-factor of 6000, $\tau = 4.9$ ps can be calculated by Eq. (6) at 1550 nm. A corresponding 3 dB bandwidth of 32 GHz is sufficient for high-speed modulation. Here we note that in small radius rings, the modulation speed is normally RC-limited because of a small Q-factor [5]. Because the HDR allows contacts of much lower resistance, this 3 μm radius HDR becomes τ-limited, which has overcome the bottleneck of electrical characteristics. For the 2 μm radius HDR, the bandwidth improvement will be more significant, exceeding a 50 GHz 3 dB bandwidth if good ohmic contact can be formed.

$$\tau = \frac{\lambda Q}{2\pi c} f_{3\,\mathrm{dB}}^2 = \frac{1}{(2\pi\tau)^2 + (2\pi RC)^2}. \tag{6}$$

Additionally, the thickness of contact layers 80/60/80 nm is not a strict requirement. The intrinsic region is simply to isolate P+ from N+. Because of the large contact area, 30 nm thickness variations of the layers will not substantially impair the electrical performance.

This work proposed a new type of resonator named a single-mode half-disk resonator, with numerical and experimental results demonstrated. Its low loss feature is characterized by an internal Q-factor of 10^5 and a loaded Q-factor of ~9000 with half of the resonator to form electrical or mechanical contacts. A 36-nm uncorrupted FSR is measured in the experiment, confirming a single-mode operation. The simulation results are proven to match well with the experimental measurements. A vertical PN junction modulator with much smaller resistance is thus enabled by the proposed device, achieving only ~50 Ω, an order of magnitude lower than previous works. The proposed HDR is a promising candidate in optical interconnection and communication.

This work is partially supported by the Major International (Regional) Cooperation and Exchange Program of the National Natural Science Foundation of China (No. 61120106012).

References

1. G. T. Reed, G. Mashanovich, F. Y. Gardes, and D. J. Thomson, Nat. Photonics **4**, 518 (2010).
2. Z. Zhou, Z. Tu, B. Yin, W. Tan, L. Yu, H. Yi, and X. Wang, Chin. Opt. Lett. **11**, 12501 (2013).
3. M. R. Watts, W. A. Zortman, D. C. Trotter, R. W. Young, and A. L. Lentine, Opt. Express **19**, 21989 (2011).
4. M. R. Watts, Opt. Lett. **35**, 3231 (2010).
5. A. Biberman, E. Timurdogan, W. A. Zortman, D. C. Trotter, and M. R. Watts, Opt. Express **20**, 29223 (2012).
6. D. Dai and J. E. Bowers, "Silicon-based on-chip multiplexing technologies and devices for petabit optical interconnects," Nanophotonics, doi: 10.1515/nanoph-2013-0021.
7. J. Liu, R. Camacho-Aguilera, J. T. Bessette, X. Sun, X. Wang, Y. Cai, L. C. Kimerling, and J. Michel, Thin Solid Films **520**, 3354 (2012).
8. D. A. B. Miller, Opt. Express **20**, A293 (2012).
9. M. Fujita and T. Baba, Appl. Phys. Lett. **80**, 2051 (2002).
10. S. A. Backes, J. R. A. Cleaver, A. P. Heberle, J. J. Baumberg, and K. Köhler, Appl. Phys. Lett. **74**, 176 (1999).
11. R. L. Levien and C. Adviser-Sequin, *From Spiral to Spline: Optimal Techniques in Interactive Curve Design* (University of California, 2009).
12. T. Chen, H. Lee, J. Li, and K. J. Vahala, Opt. Express **20**, 22819 (2012).
13. Q. Xu, S. Manipatruni, B. Schmidt, J. Shakya, and M. Lipson, Opt. Express **15**, 430 (2007).
14. Q. Xu, V. R. Almeida, and M. Lipson, Opt. Lett. **30**, 2733 (2005).
15. Q. Xu, D. Fattal, and R. G. Beausoleil, Opt. Express **16**, 4309 (2008).